Tuning the Electronic Structure of $LaNiO_3$ through Alloying with Strontium to Enhance Oxygen Evolution Activity

Jishan Liu, Endong Jia, Le Wang, Kelsey A. Stoerzinger,* Hua Zhou, Chi Sin Tang, Xinmao Yin, Xu He, Eric Bousquet, Mark E. Bowden, Andrew T. S. Wee, Scott A. Chambers, and Yingge Du**

The perovskite oxide $LaNiO_3$ is a promising oxygen electrocatalyst for renewable energy storage and conversion technologies. Here, it is shown that strontium substitution for lanthanum in coherently strained, epitaxial $LaNiO_3$ films ($La_{1-x}Sr_xNiO_3$) significantly enhances the oxygen evolution reaction (OER) activity, resulting in performance at $x = 0.5$ comparable to the state-of-the-art catalyst $Ba_{0.5}Sr_{0.5}Co_{0.8}Fe_{0.2}O_{3-\delta}$. By combining X-ray photoemission and X-ray absorption spectroscopies with density functional theory, it is shown that an upward energy shift of the O 2p band relative to the Fermi level occurs with increasing x in $La_{1-x}Sr_xNiO_3$. This alloying step strengthens Ni 3d–O 2p hybridization and decreases the charge transfer energy, which in turn accounts for the enhanced OER activity.

The electrolytic decomposition of earth-abundant H_2O, consisting of the oxygen evolution and hydrogen evolution half-cell reactions, holds significant promise for generating clean H_2 fuel.[1] However, the slow kinetics of the oxygen evolution reaction (OER) limits the efficiency of the overall process. ABO_3-type perovskite oxides are attractive electrocatalysts for promoting the OER in alkaline environments,[2–4] in that their activities are comparable to those of benchmark catalysts such as RuO_2 and IrO_2, both of which employ expensive and scarce metals.[3]

Dr. J. Liu
State Key Laboratory of Functional Materials for Informatics
Shanghai Institute of Microsystem and Information Technology
Chinese Academy of Sciences
Shanghai 200050, China

Dr. J. Liu
Center for Excellence in Superconducting Electronics
Chinese Academy of Sciences
Shanghai 200050, China

Dr. J. Liu, E. Jia, Dr. L. Wang, Prof. K. A. Stoerzinger,
Dr. S. A. Chambers, Dr. Y. Du
Physical and Computational Sciences Directorate
Pacific Northwest National Laboratory
Richland, WA 99354, USA
E-mail: le.wang@pnnl.gov; kelsey.stoerzinger@oregonstate.edu;
yingge.du@pnnl.gov

E. Jia
The Key Laboratory of Solar Thermal Energy and Photovoltaic System
Institute of Electrical Engineering
Chinese Academy of Sciences
Beijing 100190, China

E. Jia
Department of Physics
University of Chinese Academy of Sciences
Beijing 100190, China

The ORCID identification number(s) for the author(s) of this article can be found under https://doi.org/10.1002/advs.201901073.

DOI: 10.1002/advs.201901073

Prof. K. A. Stoerzinger
School of Chemical
Biological and Environmental Engineering
Oregon State University
Corvallis, OR 97331, USA

Dr. H. Zhou
X-Ray Science Division
Advanced Photon Source
Argonne National Laboratory
Lemont, IL 60439, USA

C. S. Tang, Dr. X. Yin, Prof. A. T. S. Wee
Department of Physics
Faculty of Science
National University of Singapore
Singapore 117542, Singapore

C. S. Tang
NUS Graduate School for Integrative Sciences and Engineering
National University of Singapore
Singapore 117456, Singapore

Dr. X. He, Dr. E. Bousquet
Theoretical Materials Physics
Q-MAT
Cesam
University of Liège
B-4000 Liège, Belgium

Dr. M. E. Bowden
Environmental Molecular Sciences Laboratory
Pacific Northwest National Laboratory
Richland, WA 99354, USA

The OER activity of perovskite oxides is strongly dependent on their electronic structure, and many studies have focused on identifying activity descriptors based on the electronic properties of the surface or bulk.[3–8] These descriptors span from molecular orbital based models to band theory and include the number of d electrons,[9] e_g orbital filling,[3,10] metal 3d–oxygen 2p hybridization,[11] the position of the oxygen p band center relative to the Fermi level (E_F),[2,12] and charge transfer energy (Δ).[5] Some studies suggest that the chemical properties of perovskite oxides are controlled by the metal 3d band filling.[2,13] Previous calculations show that a lower metal 3d band center weakens the metal–oxygen chemisorption energy,[13] which is believed to be favorable for enhanced OER activity.[2] Others have taken a more localized approach, focusing on e_g orbital filling in the B-site transition metal cation. In this paradigm, an e_g occupancy slightly greater than unity is considered optimal for OER.[3] However, in comparing materials with similar e_g occupancies, significant differences in OER activities still exist,[3,14] underscoring the importance of considering the nature of metal–oxygen orbital overlap in descriptions of oxygen electrocatalysis. Recently, the charge transfer energy Δ, which is the energy difference between the oxygen 2p and metal 3d orbital energies, was proposed as a key electronic descriptor for OER activity.[5]

Perovskite-structured nickelates, in particular $LaNiO_3$ (LNO), have attracted considerable attention for their desirable OER performance.[3] Various approaches including strain engineering,[2,15] cation nonstoichiometry controlling[16] have been explored in pursuit of enhancing the OER activity of nickelates. Aliovalent substitution of Sr^{2+} or Ba^{2+} for A-site La^{3+} in $LaMO_3$ (M = Co, Fe),[6,7,17–19] has been demonstrated to be an effective approach for enhancing OER activity. Recently, Sankannavar et al.[20] reported that Sr-doped LNO powders show significantly higher OER activity than pure LNO. However, according to the e_g occupancy design principle,[3] $La_{1-x}Sr_xNiO_3$ (LSNO) formation would essentially reduce the e_g orbital occupancy to less than unity, which can be unfavorable for OER.[2,3] It is thus important to examine this discrepancy to elucidate how electronic structure and OER activity of $La_{1-x}Sr_xNiO_3$ evolve as a function of x.

We have synthesized a set of compositionally and structurally well-defined epitaxial LSNO films over the full range of compositions and have investigated the resulting properties to establish the impact of Sr alloying on LSNO electronic structure and OER activity. The films were deposited using oxygen plasma–assisted molecular beam epitaxy (OPA-MBE). In contrast to previous studies of LSNO particles,[20] these epitaxial films have controlled surface areas and orientations, and are free of secondary phases such as NiO and $SrCO_3$. These films are thus ideally suited for fundamental investigations to reveal the underlying mechanisms. In-plane transport measurements confirm that the LSNO films become insulating when x exceeds 0.5 (Figure S1, Supporting Information). Due to the large potential voltage drop across the films, we cannot reliably measure OER activity for $La_{0.25}Sr_{0.75}NiO_3$ and $SrNiO_{3-\delta}$. However, within the measurable range ($0 \le x \le 0.5$), the OER

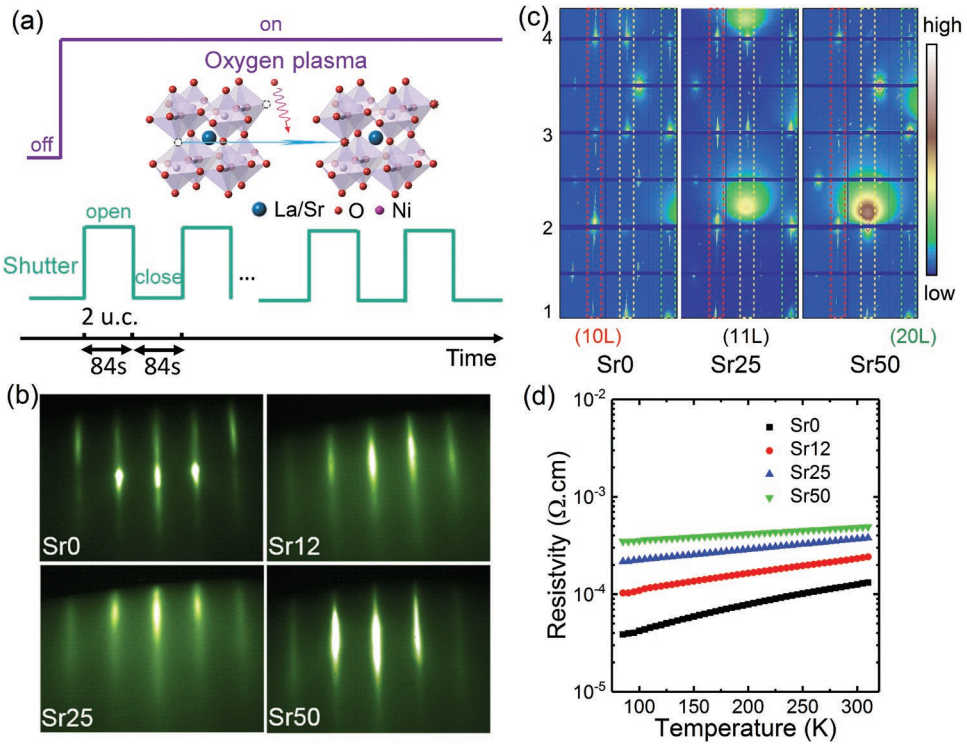

Figure 1. a) Schematic illustration of the controlled growth of LSNO films by OPA-MBE. Every 2 u.c. deposition (shutter open) was followed by an 84 s in situ annealing (shutter close) in activated oxygen. The inset schematic diagram illustrates that the oxygen vacancies can be healed by the oxygen annealing. b) RHEED patterns for LSNO films grown on LAO viewed along the [100] zone axis. $LaNiO_3$ is referred to as "Sr0," $La_{0.88}Sr_{0.12}NiO_3$ as "Sr12," $La_{0.75}Sr_{0.25}NiO_3$ as "Sr25," and $La_{0.5}Sr_{0.5}NiO_3$ as "Sr50." c) Reciprocal space mapping for the crystal truncation rods of LSNO films. The broad spot comes from parasitic scattering of W stripes used to block the extremely strong substrate Bragg peaks. d) Resistivity versus temperature on warming for LSNO films on LAO substrates.

activity is found to increase with x, with $x = 0.5$ being the most active. By combining X-ray photoemission spectroscopy (XPS) and X-ray absorption spectroscopy (XAS) with density functional theory (DFT) calculations, we show that increasing the Sr mole fraction in LSNO system induces an upward shift of the O 2p bands relative to the Fermi level, strengthening Ni 3d–O 2p hybridization, and decreasing Δ, which accounts for the enhanced OER activity.

Epitaxial LSNO films of thickness equal to 20 unit cells (u.c.) were grown on (001)-oriented $LaAlO_3$ (LAO) substrates by OPA-MBE.[21,22] Bulk LNO exhibits a rhombohedral structure with a room-temperature pseudocubic lattice constant of ≈3.84 Å.[23] LAO with its pseudocubic lattice constant of ≈3.794 Å was used as the substrate because of its small in-plane lattice mismatch with LNO. **Figure 1**a shows a schematic illustration of the alternating deposition and annealing approach to grow these LSNO films. The elemental fluxes for La, Sr, and Ni were calibrated using a quartz crystal oscillator positioned at the sample growth location. During growth, activated oxygen from an electron cyclotron plasma source operating at 40 W and a pressure of 5×10^{-6} Torr was used to achieve higher oxidizing power than that achievable with molecular oxygen (O_2). In addition, all samples were annealed in activated oxygen for 84 s at 650 °C after the growth of each 2 u.c. increment (which also required 84 s to deposit) by programming the source shutters. The samples are designated Sr0, Sr12, Sr25, and Sr50 for x values of 0, 0.12, 0.25, and 0.5, respectively. Figure 1b shows the reflection high-energy electron diffraction (RHEED) patterns for the as-grown LSNO films. RHEED is a powerful in situ technique used to characterize the surface structure of crystalline materials. These patterns exhibit sharp, bright, unmodulated streaks and no extra diffraction spots, demonstrating excellent crystallinity, smooth surface morphology, and no secondary phases. Atomic force microscope measurements further confirmed flat surfaces with root-mean square roughness ≈0.2 nm for these LSNO films (Figure S2, Supporting Information). Figure 1c shows crystal truncation rod maps from high-energy X-ray surface diffraction.[24] Bragg spots for the films are aligned with and overlap the substrates peaks, indicating coherent epitaxial growth with the same crystal orientation as the LAO. Keissig fringes are clearly seen along with the main Bragg diffraction rods for all films, demonstrating a well-defined lattice spacing with sharp interfaces and flat surfaces. Only an $a^-a^-a^-$ type octahedral rotation pattern, propagated from the substrate, is observed.[25] No extra a^+ or b^+ type rotation is seen, even for the highest x values. These results demonstrate that phase pure LSNO of high structural quality grow without secondary phase formation. Figure 1d shows resistivity versus temperature for the LSNO film series. All samples exhibit metallic behavior over the entire temperature range measured.

We now consider the effect of Sr substitution for La on OER activity. LSNO films were electrically contacted on the front and OER activity was measured using a standard three-electrode configuration in O_2 saturated 0.1 M potassium hydroxide (KOH) solution.[14] **Figure 2**a and Figure S3 (Supporting Information) show cyclic voltammetry (CV) curves to assess OER activity and

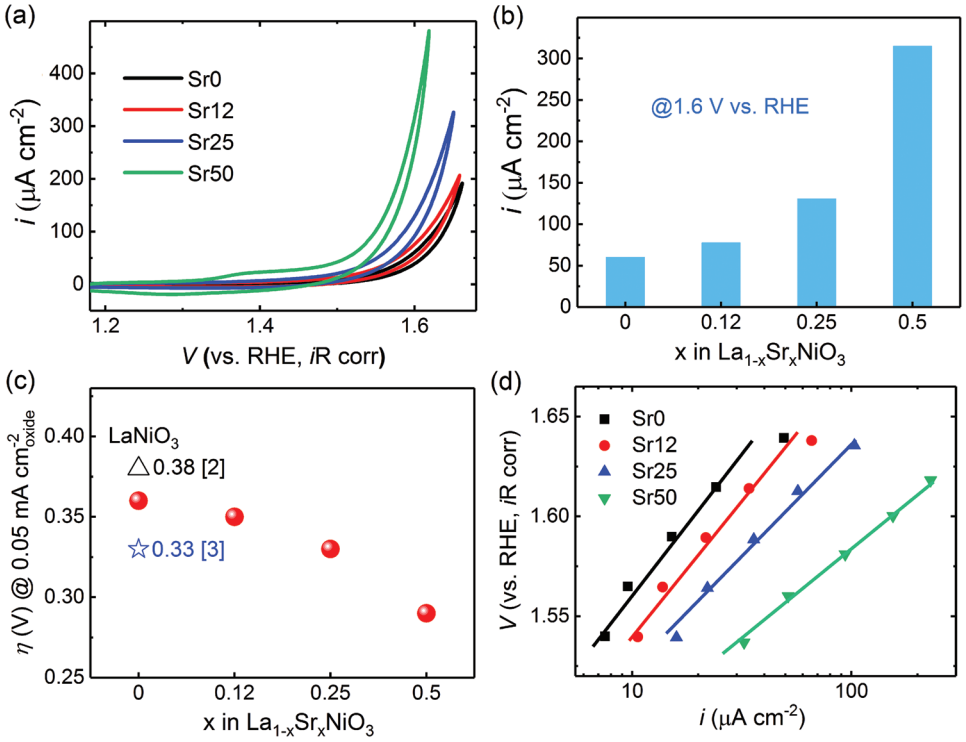

Figure 2. a) Cyclic voltammetry (CV) of LSNO films measured in O_2 saturated 0.1 M KOH at a scan rate of 10 mV s^{-1}, normalized by the specific area with voltage corrected for the electrolyte resistance. b) A comparison of the specific OER activities (current density at 1.6 V vs RHE) of LSNO films. c) Overpotentials (η) for LSNO films as required to obtain 0.05 mA cm^{-2}_{oxide} in CV measurements. The η values of $LaNiO_3$ reported from the literature are also plotted for comparison. The numbers in brackets are the citation numbers. d) Tafel plot of the OER activities of LSNO films. Points are obtained from steady state measurements by chronoamperometry, with lines as guides to the eye.

reveal a clear trend toward enhanced activity with increasing x. The specific activities (current density at 1.6 V vs the reversible hydrogen electrode (RHE)) are presented in Figure 2b. It is clear that Sr^{2+} substitution for La^{3+} is favorable for OER, with Sr50 exhibiting 315 μA cm^{-2}_{oxide}, five higher than that for Sr0 (61 μA cm^{-2}_{oxide}). For further quantitative comparison, we define the potential required to reach a current density of 50 μA cm^{-2}_{oxide}, as the OER onset potential (E_{OER}),[3,17] and calculate the overpotential (η) according to the formula $\eta = E_{OER} - 1.23$ V. We summarize the η values for our LSNO films as well as those from other previous studies of pure LNO using the same metric in Figure 2c. For pure LNO, our Sr0 sample shows a η value of ≈0.36 V, similar to those from previous studies.[2,3] As x increases from 0 to 0.5, η continuously decreases, and Sr50 exhibits the smallest η value at 0.29 V, comparable to that of the state-of-the-art catalyst $Ba_{0.5}Sr_{0.5}Co_{0.8}Fe_{0.2}O_{3-\delta}$.[3] The Tafel plots for our LSNO films shown in Figure 2d display a clear decrease in Tafel slope for higher x. The larger increase in current density for a given change in overpotential reveals favorable kinetics and efficient charge transfer at the higher x values. Previous consideration of LNO employing Marcus theory with experimentally determined electron affinity and hydroxide affinity have shown that the potentially limiting −O to −OOH step proceeds through a decoupled electron-then-proton transfer process,[5] which coupled with the present decrease in Tafel slopes with Sr suggest that electron transfer is not limiting in the LSNO system. Moreover, Figure 2a shows that the addition of Sr causes an increase in the current associated with the oxidation (1.4 V) and reduction (1.3 V) of nickel. Note that while the current from CV is similar in each cycle for low Sr content, activity increases with cycling for higher Sr content (Figure S3, Supporting Information). For better understanding of this trend, more investigation in our labs by ambient pressure X-ray photoelectron spectroscopy to probe the surface chemistry in situ and by extensive OER testing under different pH environments are still ongoing.

As shown in Figure 1d, LNO (Sr0) shows the most conductive behavior. However, Sr0 is not the most OER active. This result is in contrast to previous studies of $La_{1-x}Sr_xCoO_3$, where OER activity increased with conductivity.[19] While the parent $LaNiO_3$ is metallic, $LaCoO_3$ is insulating. Conductivity is proportional to the product of mobility and carrier concentration. For the $La_{1-x}Sr_xCoO_3$ system, Sr doping increases the carrier concentration, leading to an increase in conductivity. But for $La_{1-x}Sr_xNiO_3$, Sr doping may increase the carrier density, but it will also decrease the mobility due to the increase of ionized impurity scattering. The product of these two effects induces a decrease in conductivity. In order to better understand the relationship between OER activity and electronic structure, we performed XAS and XPS measurements at room temperature to probe the unoccupied and occupied electronic states, respectively. **Figure 3**a and Figure S4 (Supporting Information) show the normalized O K-edge XAS pre-edge features for the film series. The peaks fall at ≈528 eV, and correspond to a transition from the O 1s core to the lowest unoccupied hybridized O 2p–Ni 3d band. We designate this transition as $3d^8\underline{L} \rightarrow c3d^8$ where $\underline{L}$ and c denote a hole in the O 2p ligand orbital and an O 1s core hole, respectively.[26–28] The O K prepeak width can be used to measure the degree of O 2p–Ni 3d hybridization as

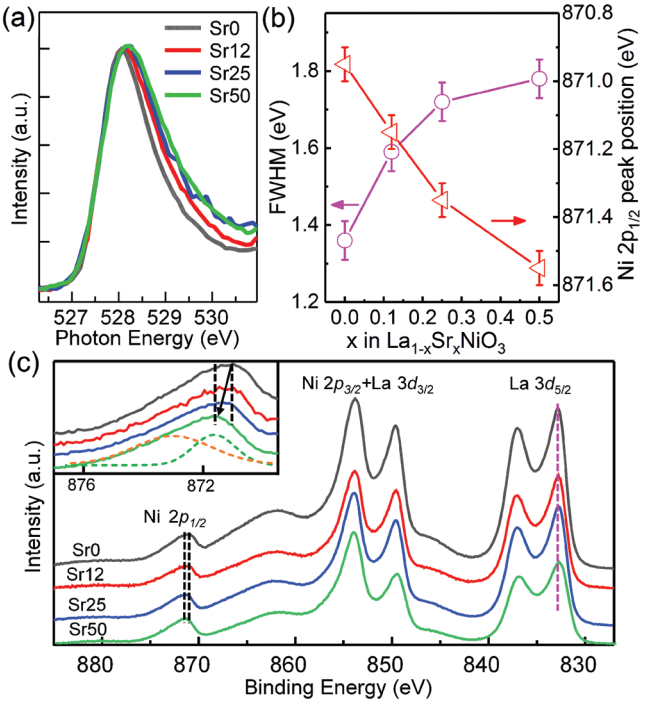

Figure 3. a) Soft X-ray absorption O K pre-edge spectra for LSNO films taken at 300 K. b) O K prepeak full width at half maximum (FWHM) values near 528 eV and Ni $2p_{1/2}$ peak energies extracted from (c) versus x. c) La 3d and Ni 2p XPS measured in situ for the LSNO film series. All spectra are shifted so the associated O 1s peaks fall at 530.0 eV. As a guide to the eye, we mark the La $3d_{5/2}$ peak position with a magenta dashed line. Inset: Ni $2p_{1/2}$ spectra for which the peak shift with x is clearly seen. These asymmetric peaks were fit to a pair of model functions (dashed curves) solely for the purpose of tracking changes in the binding energy with x, as plotted in panel (b).

it is related to the Ni−O−Ni bond angle, as has been well elucidated in previous studies.[29–31] Figure 3a,b shows that the O K pre-edge peak width increases with increasing x, suggesting an increase in Ni 3d–O 2p hybridization. According to previous studies,[3,32] the OER activity is strongly related to the ability of the electrocatalyst surface to bind oxygen. The reaction intermediates, including *OH, *O, *OOH, interact with the catalyst surface through the oxygen atom.[33] Enhanced Ni 3d–O 2p hybridization can improve electron extraction from oxygen adsorbates, thus increasing the OER activity.[11] Note that this enhancement of Ni 3d–O 2p hybridization may result from the increase of Ni oxidation state by Sr^{2+} substitution. Our in situ XPS measurements (Figure 3c and Figure S5 (Supporting Information)) indeed reveal a shift of the Ni $2p_{1/2}$ peak to the higher binding energy with increasing x, suggesting an increase in Ni valence. While the elusive Ni^{4+} is difficult to pinpoint spectroscopically, the X-ray diffraction (XRD) data suggest its existence as follows. Sr^{2+} has a larger ionic radius than La^{3+} (1.26 vs 1.16 Å),[34] thus the lattice parameters of LSNO should increase as x increases. However, as shown in Figure 1c and Figure S6 (Supporting Information), the lattice parameter becomes smaller with Sr doping, which can only be rationalized by Ni^{4+} creation. The smaller ionic radius of Ni^{4+} would shorten the Ni−O bond length, leading to the enhancement of covalency or Ni 3d–O 2p hybridization.

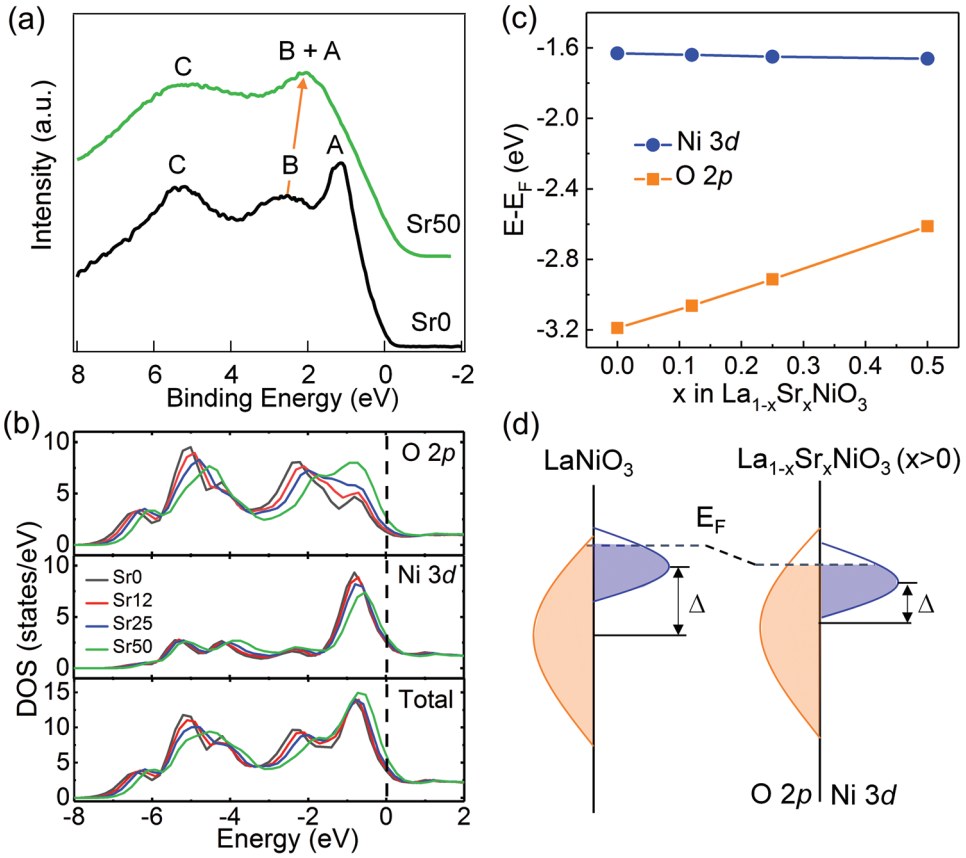

Figure 4. a) XPS VB spectra for Sr0 and Sr50. b) Computed partial and total densities of states from DFT. The black dashed line denotes E_F. c) Average onsite energies of O 2p and Ni 3d orbitals with E_F as the reference. d) Schematic energy band diagram for $LaNiO_3$ and $La_{1-x}Sr_xNiO_3$ ($x > 0$), where Δ is the charge transfer energy.

The enhancement in hybridization is also reflected in the evolution of the valence band (VB). A clear upward shift of the O 2p band is observed in our XPS measurements (**Figure 4**a) and DFT calculations (Figure 4b). For pure LNO (Sr0), the VB spectrum consists of three features labeled as A, B, and C. By contrast, Sr50 exhibits only two distinct components as features A and B merge. According to our DFT calculations (Figure 4b) and previous reports,[35,36] feature A is assigned to a predominantly occupied Ni 3d band with minor O 2p character. Feature B arises primarily from O—O interactions and is assigned to the nonbonding O 2p band with only a small covalent admixture of Ni 3d, whereas feature C is assigned to bonding states. The experimental spectra are in good agreement with our DFT calculations; the O 2p band shifts upward in energy and moves close to E_F, inducing mixing of features A and B, as observed in the VB spectra for Sr50 (Figure 4a). The merging of features A and B is due not only to the reduced spacing between the two peaks, but also to the fact the antibonding state has more O 2p character than the nonbonding state with enhanced Ni 3d–O 2p hybridization (Figure 4b). Figure 4c shows the computed average onsite energies of the O 2p and Ni 3d bands relative to E_F. With increasing x, O 2p bands shift up and move closer to E_F. The upshift of the O 2p bands, which enhances Ni 3d–O 2p hybridization (covalency), is due to the decrease in Coulomb interaction with the A site cation when the valence of the latter changes from 3+ to 2+. Viewed from a different perspective, Sr^{2+} substitution for La^{3+} results in hole doping in LNO, driving a downward shift in E_F relative to pure LNO. As the O 2p band center shifts upward and approaches E_F, the antibonding states below E_F exhibit greater oxygen character, which in turn promotes electron transfer to and from oxygen by allowing Ni 3d to mix more strongly with O 2p, thus leading to higher OER activity. We note that a shift of the O 2p band closer to the Fermi level leads to activation during cycling in Co oxides[12] and the formation of an amorphous Co oxide layer,[37] and while LNO's O 2p band center is low enough such change is unexpected, the increase with Sr content could trigger such a structural change during OER. However, changes in LSNO film capacitance with cycling was not observed, suggesting that the electrochemical surface area remains unchanged with cycling.

In perovskite transition metal oxides, the extent of metal 3d–oxygen 2p hybridization scales with the ratio of the transfer integral to charge transfer energy (Δ).[38] For nickelates, the Ni 3d–O 2p hybridization is primarily controlled by Δ, while the transfer integral has a weaker influence.[36] The evolution of Ni 3d and O 2p bands revealed in our VB measurements and DFT calculations confirm the decrease in Δ with increasing x as a result of stronger hybridization. Based on the above analysis, we show a schematic energy band diagram (Figure 4d) for pure LNO and LSNO ($x > 0$). The decrease in Δ should enhance OER

activity as x increases. Hole doping of the O 2p band can lead to more effective electronic screening at the surface, decreasing the barrier for the electron transfer step of the OER.[5]

In summary, we have demonstrated that Sr^{2+} substitution for La^{3+} in $LaNiO_3$ is an effective way to improve OER activity. The combination of experimental results with DFT calculations demonstrates that synthesizing this solid solution reduces the charge transfer energy and strengthens Ni 3d–O 2p hybridization, which in turn leads to higher OER activity. At $x = 0.5$ ($La_{0.5}Sr_{0.5}NiO_3$), the overpotential required to achieve 50 μA cm^{-2}_{oxide} is 0.29 V, which is comparable to that of the state-of-the-art catalyst $Ba_{0.5}Sr_{0.5}Co_{0.8}Fe_{0.2}O_{3-\delta}$. Our study offers new insights into the effect of solid solution formation on OER activity in perovskite nickelates and will promote the application of this solid-state chemistry to make effective oxygen electrocatalysts.

Supporting Information

Supporting Information is available from the Wiley Online Library or from the author.

Acknowledgements

This work was supported by the U. S. Department of Energy (DOE), Office of Science, Early Career Research Program under Award #68272. XRD and XPS analysis were supported by the U.S. DOE, Office of Science, Office of Basic Energy Sciences, the Division of Materials Sciences and Engineering under Award #10122. Electrochemical measurements were supported for K.A.S. by the Linus Pauling Distinguished Postdoctoral Fellowship at the Pacific Northwest National Laboratory (PNNL LDRD69319). J.L. was supported by the China Scholarship Council (CSC) as a visiting scholar at the Pacific Northwest National Laboratory. This research used resources of the Advanced Photon Source, a U.S. Department of Energy (DOE) Office of Science User Facility operated for the DOE Office of Science by Argonne National Laboratory under Contract No. DE-AC02-06CH11357. This article has been contributed to by US Government employees and their work is in the public domain in the USA. The authors thank Dr. John Okasinski from the Advanced Photon Source for the support and also thank the Singapore Synchrotron Light Source (SSLS) for providing the facilities support. X.H. and E.B. acknowledge the ARC AIMED project and the CECI facilities funded by FRS-FNRS (Grant No. 2.5020.1). A portion of the research was performed using EMSL (grid. 436923.9), a DOE Office of Science User Facility sponsored by the Office of Biological and Environmental Research. PNNL is a multiprogram national laboratory operated for DOE by Battelle.

Conflict of Interest

The authors declare no conflict of interest.

Keywords

hole doping, hybridization, $LaNiO_3$, nickelates, oxygen evolution reaction

Received: May 7, 2019
Revised: July 17, 2019
Published online: August 7, 2019

[1] Z. W. Seh, J. Kibsgaard, C. F. Dickens, I. Chorkendorff, J. K. Norskov, T. F. Jaramillo, *Science* **2017**, *355*, eaad4998.
[2] J. R. Petrie, V. R. Cooper, J. W. Freeland, T. L. Meyer, Z. Zhang, D. A. Lutterman, H. N. Lee, *J. Am. Chem. Soc.* **2016**, *138*, 2488.
[3] J. Suntivich, K. J. May, H. A. Gasteiger, J. B. Goodenough, Y. Shao-Horn, *Science* **2011**, *334*, 1383.
[4] J. Hwang, R. R. Rao, L. Giordano, Y. Katayama, Y. Yu, Y. Shao-Horn, *Science* **2017**, *358*, 751.
[5] W. T. Hong, K. A. Stoerzinger, Y.-L. Lee, L. Giordano, A. Grimaud, A. M. Johnson, J. Hwang, E. J. Crumlin, W. Yang, Y. Shao-Horn, *Energy Environ. Sci.* **2017**, *10*, 2190.
[6] J. T. Mefford, X. Rong, A. M. Abakumov, W. G. Hardin, S. Dai, A. M. Kolpak, K. P. Johnston, K. J. Stevenson, *Nat. Commun.* **2016**, *7*, 11053.
[7] X. Cheng, E. Fabbri, M. Nachtegaal, I. E. Castelli, M. El Kazzi, R. Haumont, N. Marzari, T. J. Schmidt, *Chem. Mater.* **2015**, *27*, 7662.
[8] Y. Tong, Y. Guo, P. Chen, H. Liu, M. Zhang, L. Zhang, W. Yan, W. Chu, C. Wu, Y. Xie, *Chem* **2017**, *3*, 812.
[9] F. Calle-Vallejo, N. G. Inoglu, H.-Y. Su, J. I. Martínez, I. C. Man, M. T. Koper, J. R. Kitchin, J. Rossmeisl, *Chem. Sci.* **2013**, *4*, 1245.
[10] C. Wei, Z. Feng, G. G. Scherer, J. Barber, Y. Shao-Horn, Z. J. Xu, *Adv. Mater.* **2017**, *29*, 1606800.
[11] J. Suntivich, W. T. Hong, Y.-L. Lee, J. M. Rondinelli, W. Yang, J. B. Goodenough, B. Dabrowski, J. W. Freeland, Y. Shao-Horn, *J. Phys. Chem. C* **2014**, *118*, 1856.
[12] A. Grimaud, K. J. May, C. E. Carlton, Y.-L. Lee, M. Risch, W. T. Hong, J. Zhou, Y. Shao-Horn, *Nat. Commun.* **2013**, *4*, 2439.
[13] S. A. Akhade, J. R. Kitchin, *J. Chem. Phys.* **2012**, *137*, 084703.
[14] L. Wang, K. A. Stoerzinger, L. Chang, J. Zhao, Y. Li, C. S. Tang, X. Yin, M. E. Bowden, Z. Yang, H. Guo, *Adv. Funct. Mater.* **2018**, *28*, 1803712.
[15] L. Wang, K. A. Stoerzinger, L. Chang, X. Yin, Y. Li, C. S. Tang, E. Jia, M. E. Bowden, Z. Yang, A. Abdelsamie, *ACS Appl. Mater. Interfaces* **2019**, *11*, 12941.
[16] J. Bak, H. B. Bae, J. Kim, J. Oh, S.-Y. Chung, *Nano Lett.* **2017**, *17*, 3126.
[17] S. Yagi, I. Yamada, H. Tsukasaki, A. Seno, M. Murakami, H. Fujii, H. Chen, N. Umezawa, H. Abe, N. Nishiyama, *Nat. Commun.* **2015**, *6*, 8249.
[18] S. She, J. Yu, W. Tang, Y. Zhu, Y. Chen, J. Sunarso, W. Zhou, Z. Shao, *ACS Appl. Mater. Interfaces* **2018**, *10*, 11715.
[19] K. A. Stoerzinger, X. R. Wang, J. Hwang, R. R. Rao, W. T. Hong, C. Rouleau, D. Lee, Y. Yu, E. J. Crumlin, Y. Shao-Horn, *Top. Catal.* **2018**, *61*, 2161.
[20] R. Sankannavar, K. Sandeep, S. Kamath, A. K. Suresh, A. Sarkar, *J. Electrochem. Soc.* **2018**, *165*, J3236.
[21] R. Comes, S. Chambers, *Phys. Rev. Lett.* **2016**, *117*, 226802.
[22] L. Wang, Y. Du, L. Chang, K. Stoerzinger, M. Bowden, J. Wang, S. Chambers, *Appl. Phys. Lett.* **2018**, *112*, 261601.
[23] A. S. Disa, D. Kumah, J. Ngai, E. D. Specht, D. Arena, F. J. Walker, C. H. Ahn, *APL Mater.* **2013**, *1*, 032110.
[24] J. Gustafson, M. Shipilin, C. Zhang, A. Stierle, U. Hejral, U. Ruett, O. Gutowski, P.-A. Carlsson, M. Skoglundh, E. Lundgren, *Science* **2014**, *343*, 758.
[25] S. J. May, J. W. Kim, J. M. Rondinelli, E. Karapetrova, N. A. Spaldin, A. Bhattacharya, P. J. Ryan, *Phys. Rev. B* **2010**, *82*, 014110.
[26] P. Kuiper, G. Kruizinga, J. Ghijsen, G. Sawatzky, H. Verweij, *Phys. Rev. Lett.* **1989**, *62*, 221.
[27] M. Abbate, G. Zampieri, F. Prado, A. Caneiro, J. Gonzalez-Calbet, M. Vallet-Regi, *Phys. Rev. B* **2002**, *65*, 155101.
[28] N. Palina, L. Wang, S. Dash, X. Yu, M. B. Breese, J. Wang, A. Rusydi, *Nanoscale* **2017**, *9*, 6094.
[29] S. Middey, D. Meyers, S. K. Ojha, M. Kareev, X. Liu, Y. Cao, J. Freeland, J. Chakhalian, *Phys. Rev. B* **2018**, *98*, 045115.
[30] J. Liu, M. Kargarian, M. Kareev, B. Gray, P. J. Ryan, A. Cruz, N. Tahir, Y.-D. Chuang, J. Guo, J. M. Rondinelli, *Nat. Commun.* **2013**, *4*, 2714.

[31] J. Chakhalian, J. Rondinelli, J. Liu, B. Gray, M. Kareev, E. Moon, N. Prasai, J. Cohn, M. Varela, I.-C. Tung, *Phys. Rev. Lett.* **2011**, *107*, 116805.
[32] D.-Y. Kuo, C. J. Eom, J. K. Kawasaki, G. Petretto, J. N. Nelson, G. Hautier, E. J. Crumlin, K. M. Shen, D. G. Schlom, J. Suntivich, *J. Phys. Chem. C* **2018**, *122*, 4359.
[33] I. C. Man, H. Y. Su, F. Calle-Vallejo, H. A. Hansen, J. I. Martínez, N. G. Inoglu, J. Kitchin, T. F. Jaramillo, J. K. Nørskov, J. Rossmeisl, *ChemCatChem* **2011**, *3*, 1159.
[34] R. D. Shannon, *Acta Crystallogr., Sect. A: Found. Adv.* **1976**, *32*, 751.
[35] D. Sarma, N. Shanthi, P. Mahadevan, *J. Phys.: Condens. Matter* **1994**, *6*, 10467.
[36] S. Barman, A. Chainani, D. Sarma, *Phys. Rev. B* **1994**, *49*, 8475.
[37] M. Risch, A. Grimaud, K. J May, K. A Stoerzinger, T. J Chen, A. N Mansour, Y. Shao-Horn, *J. Phys. Chem. C* **2013**, *117*, 8628.
[38] M. N. Grisolia, J. Varignon, G. Sanchez-Santolino, A. Arora, S. Valencia, M. Varela, R. Abrudan, E. Weschke, E. Schierle, J. E. Rault, J. P. Rueff, A. Barthelemy, J. Santamaria, M. Bibes, *Nat. Phys.* **2016**, *12*, 484.